



**HAL**  
open science

# The Impact of Iron Oxide Concentration on the Performance of Molten Oxide Electrolytes for the Production of Liquid Iron Metal

Jan Wiencke, Hervé Lavelaine, Pierre-Jean Panteix, Carine Petitjean, Christophe Rapin

## ► To cite this version:

Jan Wiencke, Hervé Lavelaine, Pierre-Jean Panteix, Carine Petitjean, Christophe Rapin. The Impact of Iron Oxide Concentration on the Performance of Molten Oxide Electrolytes for the Production of Liquid Iron Metal. Metallurgical and Materials Transactions B, 2020, 51 (1), pp.365-376. <10.1007/s11663-019-01737-3>. <hal-04010934>

**HAL Id: hal-04010934**

**<https://hal.science/hal-04010934v1>**

Submitted on 2 Mar 2023

HAL is a multi-disciplinary open access archive for the deposit and dissemination of scientific research documents, whether they are published or not. The documents may come from teaching and research institutions in France or abroad, or from public or private research centers.

L'archive ouverte pluridisciplinaire HAL, est destinée au dépôt et à la diffusion de documents scientifiques de niveau recherche, publiés ou non, émanant des établissements d'enseignement et de recherche français ou étrangers, des laboratoires publics ou privés.



HAL Authorization

# The Impact of Iron Oxide Concentration on the Performance of Molten Oxide Electrolytes for the Production of Liquid Iron Metal



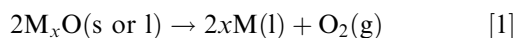
JAN WIENCKE, HERVÉ LAVELAINE, PIERRE-JEAN PANTEIX, CARINE PETITJEAN, and CHRISTOPHE RAPIN

The effect of iron oxide concentration on the conductive behavior of a molten oxide electrolyte has been investigated at 1823 K using stepped linear scan voltammetry. To maximize the current flow through the electrolyte the ohmic drop in the cell was minimized by shortening the electrode distance. The acquired current was then interpreted by means of an ohmic drop correction, taking into account the conductivity of the alumina-silicate electrolyte and the geometrical form factor of the cell. *Via* this methodology, a mass transfer limitation in dependence of the iron oxide concentration was identified. This mass transfer limitation vanishes above 7 wt pct of iron oxide where charge transfer starts to be limited solely by electrochemical reaction kinetics. In the analyzed range of concentration, an impact of iron oxide on electronic conduction was not measurable. In addition to these findings, the faradaic yield of the anode half-reaction was determined by the life-measure of O<sub>2</sub>-production. Hereby, a domain of an anodic yield close to 100 pct for various iron oxide concentrations was identified. Based on these findings, suitable conditions for the electrochemical production of liquid iron were determined.

<https://doi.org/10.1007/s11663-019-01737-3>  
© The Author(s) 2019

## I. INTRODUCTION

MOLTEN oxide electrolysis (MOE) is a promising route for metal extraction from its oxide ore.<sup>[1]</sup> Products obtained are O<sub>2</sub> gas at the anode and metal at the cathode



The possibility to produce metal samples using this technique has been addressed by several authors.<sup>[2–8]</sup> As known for aluminum production, the advantage of metal production at liquid state is given by facile recovery of the produced metal and continuous operation.<sup>[9]</sup> The use of electricity for metal extraction also implies the possibility for the usage of renewable

energies and thus the decoupling of metal production from CO<sub>2</sub> emissions. Therefore, this technology marks a major interest for steel industry, if applicable to industrial scales of production.<sup>[10,11]</sup>

Presence of multivalent elements, such as iron, at high concentration allows electronic and ionic conduction to occur simultaneously in the molten oxide electrolyte.<sup>[12]</sup> For an operation at a high faradaic yield, current flow has to occur entirely *via* ionic conduction. The participation of electronic conduction in the overall conduction is mainly dependent on the ratio of the multivalent species. For iron this value, the ferric ratio, is given *via*:

$$\text{Ferric ratio} = \frac{Fe^{(III)}}{Fe^{(II)} + Fe^{(III)}} \quad [2]$$

with Fe<sup>(II)</sup> and Fe<sup>(III)</sup> being the respective molar quantities. It was shown that current flow by electronic conduction in molten oxides is dominant if the ferric ratio is in the range of 0.25 to 0.75.<sup>[13,14]</sup> The ferric ratio itself is coupled to the temperature, to the partial pressure of oxygen,<sup>[15]</sup> to the basicity of the molten oxide<sup>[16]</sup> and to the concentration of iron oxide.<sup>[17]</sup> An experimental approach, “Molten Iron by Direct Electrolysis of Iron Ore”—MIDEIO, in which the ferric ratio was decreased to a minimum, has confirmed recently the feasibility of the liquid iron metal by electrolysis of iron oxide in molten silicates.<sup>[18]</sup>

JAN WIENCKE is with the Department of Ironmaking, Global Research and Development ArcelorMittal, 57283 Maizières-lès-Metz, France and also with the Département CP2S, Université de Lorraine, IJL-UMR 7198, 54000 Nancy, France. Contact e-mail: Jan.wiencke@arcelormittal.com HERVÉ LAVELAINE is with the Department of Ironmaking, Global Research and Development ArcelorMittal. PIERRE-JEAN PANTEIX, CARINE PETITJEAN, and CHRISTOPHE RAPIN are with the Département CP2S, Université de Lorraine, IJL-UMR 7198.

Manuscript submitted February 20, 2019.  
Article published online December 12, 2019.

The identification of side reactions and of resistances to current flow phenomena during electrolysis is an imperative step for further large-scale process development. Favorable operating conditions for the MIDEIO process are defined by a low electronic current contribution, a maximum current density and an anodic yield for O<sub>2</sub> production close to unity. To describe the dependence of these parameters on the iron oxide concentration, stepped linear scan voltammetry technique has been performed to establish the current voltage relation for the electrolyte proposed for MIDEIO. The experiments were carried out in a two electrode cell configuration, dedicated to the minimization of the ohmic drop in the electrolyte. The electrochemical measurements are accompanied by oxygen gas analysis, permitting a separate evaluation of the faradaic process occurring at the anode. As the acquired oxygen gas signal is an independent measurement, it can be used as an orientation towards the electrochemical potential in the cell, since the O<sub>2</sub> production is coupled to distinct thermodynamic thresholds of the electrochemical reactions. Taking into account the thermodynamic conditions and the production of O<sub>2</sub> gas, the lack of a reference electrode is compensated. The impact of iron oxide on the electrochemical behavior and key process indicators was studied in the range of 0 to 10 wt pct of iron oxide.

## II. MATERIALS AND METHODS

### A. Choice of Composition and Voltage Conditions

In the preceding study,<sup>[18]</sup> an electrolyte based on an Al<sub>2</sub>O<sub>3</sub>-MgO-SiO<sub>2</sub>, named here Fe#0, was proposed for MIDEIO. In the work presented here, various amounts of iron in the form of Fe<sub>3</sub>O<sub>4</sub> were added to this electrolyte to study its impact on the electrolyte's conductive behavior. The compositions investigated and the respective ferric ratios are given in Table I. Determination of the ferric ratio in equilibrium with the furnace atmosphere was done for each electrolyte *via* the thermochemical software CEQCSI,<sup>[19]</sup> which uses a quasichemical approach for the modeling of the molten oxide.

The relevant interval for the stepped linear scan voltammetry (SLSV) is defined by the thermodynamic redox-potentials of the different electrolyte compounds. These were determined for the different electrolyte components in pure component state using data from Barin<sup>[20]</sup> and are given in Table II.

The decomposition voltage of iron oxide is significantly lower than those of the other electrolyte compounds, suggesting a high selectivity of the process. The voltage range for MIDEIO operation is defined between the respective onsets of iron oxide and silica decomposition. However, in this study, iron oxide is strongly diluted in the electrolytes. To quantify the effect of this dilution on the decomposition voltage, the thermochemical software CEQCSI was used to determine the thermodynamic activities of ferrous iron ions in the different slag compositions at the equilibrium of iron metal. The redox-potential  $\Delta E$  for the diluted iron oxide is then calculated *via*

$$\Delta E = \frac{\Delta G^0}{nF} + \frac{RT}{nF} \ln[\prod_i a_i^{v_i}] \quad [9]$$

where  $\Delta G^0$  is the Gibbs energy of the considered reaction in pure component state (J mol<sup>-1</sup>),  $F$  Faraday's constant (C mol<sup>-1</sup>),  $\prod_i a_i^{v_i}$  is the activity product with  $v_i$  the stoichiometric coefficient of compound "i",  $n$  the number of electrons involved in the reaction,  $T$  the temperature [K] and  $R$  the universal gas constant (J mol<sup>-1</sup> K<sup>-1</sup>). Respective values for  $\Delta E$ , ferrous and ferric iron activity ( $a[\text{Fe}^{(II)}]$ - $a[\text{Fe}^{(III)}]$ ) and PO<sub>2</sub> are shown in Table III. Activities of iron metal and oxygen gas in reaction [3] are considered as unity. Despite the shift in the decomposition voltage due to dilution, an interval between the decomposition of iron- and silicon-oxides exists, thus, implying a clear domain for selective production of liquid iron metal. Taking into account the different decomposition voltages and the ohmic drop in the molten oxide, the cell voltage interval for the SLSV is defined as 0 to 3 V.

**Table II. Thermodynamic Redox-Potentials at 1823 K of Oxide Components of the Electrolyte in Pure Component State**

Reaction	Decomposition Voltage (V)
2Fe <sub>0.947</sub> O <sub>2</sub> ⇌ 1.894Fe <sup>0</sup> + O <sub>2</sub> [3]	0.77
2SiO <sub>2</sub> ⇌ 2Si <sup>0</sup> + O <sub>2</sub> [4]	1.29
SiO <sub>2</sub> ⇌ Si <sup>0</sup> + O <sub>2</sub> [5]	1.51
2SiO <sub>2</sub> ⇌ SiO + O <sub>2</sub> [6]	1.71
MgO ⇌ Mg <sup>0</sup> + O <sub>2</sub> [7]	1.84
2/3Al <sub>2</sub> O <sub>3</sub> ⇌ 4/3Al + O <sub>2</sub> [8]	1.89

**Table I. Electrolyte Compositions and the Respective Ferric Ratio**

Weight Percent	Fe#0	Fe#1	Fe#2	Fe#3.5	Fe#5	Fe#7.5	Fe#8.75	Fe#10
SiO <sub>2</sub>	66.00	65.34	64.68	63.69	62.70	61.05	60.23	59.40
Al <sub>2</sub> O <sub>3</sub>	20.00	19.80	19.60	19.30	19.00	18.50	18.25	18.00
MgO	14.00	13.86	13.72	13.51	13.30	12.95	12.78	12.60
Fe <sub>3</sub> O <sub>4</sub>	—	1.00	2.00	3.50	5.00	7.50	8.75	10.00
Ferric Ratio	—	2.9 × 10 <sup>-2</sup>	2.9 × 10 <sup>-2</sup>	3.0 × 10 <sup>-2</sup>	3.0 × 10 <sup>-2</sup>	3.1 × 10 <sup>-2</sup>	3.1 × 10 <sup>-2</sup>	3.1 × 10 <sup>-2</sup>

**Table III. Thermodynamic Decomposition Voltage at 1823 K of Iron Oxide in the Electrolyte in Dependence of Its Concentration**

Reaction [3]	Fe#1	Fe#2	Fe#3.5	Fe#5	Fe#7.5	Fe#8.75	Fe#10
$\Delta E$ [V]	1.16	1.11	1.07	1.04	1.02	1.01	1.00
$a[\text{Fe}^{(II)}]$	0.01	0.03	0.05	0.06	0.09	0.10	0.11
$a[\text{Fe}^{(III)}]$	$9 \times 10^{-9}$	$6 \times 10^{-8}$	$3 \times 10^{-7}$	$7 \times 10^{-7}$	$2 \times 10^{-6}$	$3 \times 10^{-6}$	$4 \times 10^{-6}$
$\text{PO}_2$ [Bar]	$4 \times 10^{-7}$	$7 \times 10^{-7}$	$1 \times 10^{-6}$	$2 \times 10^{-6}$	$2 \times 10^{-6}$	$3 \times 10^{-6}$	$3 \times 10^{-6}$

**Table IV. List of Chemical Substances Used for the Electrolyte**

	Supplier	Grain size	Purity (Pct)
$\text{SiO}_2$	Alfa Aesar	$\leq 10 \mu\text{m}$	99.5
$\text{Al}_2\text{O}_3$	Alfa Aesar	mm	98
$\text{MgO}$	Alfa Aesar	$\leq 100 \text{ nm}$	99 +
$\text{Fe}_3\text{O}_4$	Aldrich	$\leq 5 \mu\text{m}$	98

### B. Equipment and Experimental Conditions

The electrolyte was prepared from oxide powders. To ensure homogeneity, the base electrolyte composition, Fe#0, was prepared by two pre-melting procedures at 1873 K with a subsequent rapid quench at air on a steel plate. After each fusion the glass was milled with a planetary ball mill into powder. The respective amount of iron oxide was then added to the resulting powder mixture. Chemical sources of the different oxides are listed in Table IV.

The base of the experimental setup was constituted of a vertical tube furnace, flushed with an argon gas flow (Westfalen, Ar: 99.998 pct  $\text{O}_2$ :3 ppm). A gas flow-rate of  $0.05 \text{ m}^3 \text{ h}^{-1}$ , given at standard conditions (STP), defined for atmospheric pressure and temperature of 273.15 K, was adjusted. Experiments were performed in the isothermal region of the tube furnace in an alumina crucible into which two Pt/Rh-electrodes were inserted. Both materials were chosen due to their high temperature stability and chemical resistance toward the electrolyte.<sup>[21]</sup> Temperature was measured *via* a B-type thermocouple, positioned directly next to the cell. The resistance of the wiring in the cell and the furnace was measured in a blank trial performed at 1823 K, in which the electrodes were short-circuited, and determined at  $0.8 \Omega$ .

SLSV has been applied in the cell voltage range of 0 to 3 V with a cell voltage step interval of 100 mV. The voltage range was defined following the results previously obtained for liquid iron metal production.<sup>[18,23]</sup> Indeed, liquid iron has already been obtained after 6 hours of electrolysis at a cell voltage of 3 V in Fe#15 composition,<sup>[18]</sup> and also after performing SLSV up to 1.9 V in Fe#10 composition.<sup>[23]</sup> The step-length was 600 seconds (effective scanning rate  $0.17 \text{ mV s}^{-1}$ ). Current values in the displayed graphs are the average of the measured current values acquired during the second half of each cell voltage increment. At this point current values had generally stabilized. The electrochemical conditions were applied *via* a VersaStat 3 (Ametek) potentiostat and its joint software VersaStudio 2.41.2.

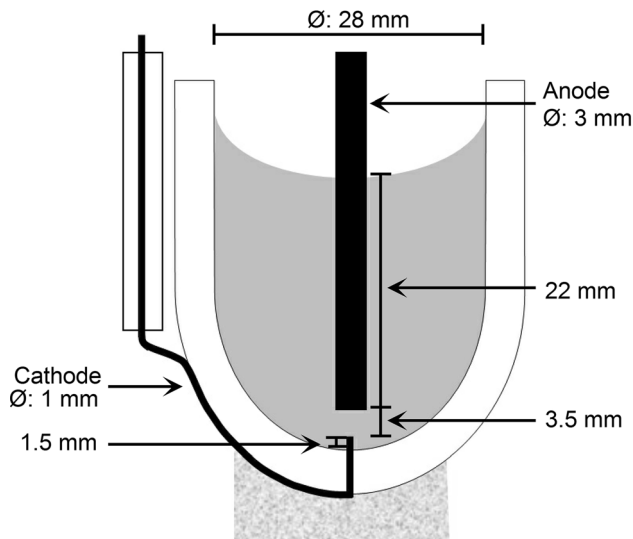


Fig. 1—Schematic drawing of the electrochemical cell.

Argumentation for the choice of materials, electrolyte composition as well as a detailed description of the experimental set-up is given elsewhere.<sup>[18]</sup>

### C. Cell Geometry and the Compensation of the Ohmic Drop

The electrochemical cell, shown in Figure 1, consists of a round-shaped bottom crucible and two vertically oriented electrodes. The cathode, a 1-mm-thick Pt-30Rh wire, is entered through the bottom of the cell and protrudes the crucible by 1.5 mm, resulting in a surface area of  $5.5 \text{ mm}^2$  in contact with the electrolyte. The anode is a 3-mm-thick Pt-10Rh rod and is immersed into the electrolyte from atop. To minimize the ohmic drop in the voltage signal, the distance between electrodes was reduced to 3.5 mm. This electrode distance is close enough to reduce the ohmic drop sufficiently, yet wide enough to allow the growth of the cathode deposit and the evolution of anodic gas bubbles. For this electrode configuration it is necessary to immerse the anode in the slag 22 mm (error of  $\pm 1 \text{ mm}$ ), which results in an immersed electrode surface of  $214 \text{ mm}^2$ . Following the variation of the molten oxide's density with different iron oxide concentrations, the immersion depth slightly changes between the different trials. Additionally, the immersion depth was affected by the diameter of the different crucibles, which is given by the manufacturer

with an error of 1 mm. Since current flow will mainly occur between the tips of the electrodes, this variation was assumed to be negligible. The ratio of the total immersed anode surface over the cathode surface is 39.

To identify resistive phenomena other than ohmic conduction, the ohmic resistance of the electrolyte,  $R_{MO}$ , must be quantified. The ohmic resistance of the electrolyte is the result of the cell geometry, expressed by the geometrical factor  $\kappa$ , and of the molten oxide's conductivity,  $\sigma_{MO}$ , and can be determined *via*:

$$R_{MO} = \frac{\kappa}{\sigma_{MO}} \quad [10]$$

The geometrical factor is obtained *via* a numerical simulation solving the Laplace equation and for the defined cell-geometry it is  $1.64 \text{ cm}^{-1}$ . Figure 2 shows the geometry of the cell together with the corresponding equipotential lines ( $V_{\text{Equi.}}$ ) and constant stream-function lines ( $\text{CSF}_{\text{Equi.}}$ ). The latter represent the current distribution in the cell. The current distribution is uniform on the cathode, while at the anode most of the current flow is concentrated at its tip, facing the cathode.

An empirical model was used to derive the conductivity of the molten oxide.<sup>[22]</sup> The corresponding results for iron oxide concentrations from 0 to 10 wt pct are shown in Table V.

To display solely the dependence of the faradaic current on the potential, the measured data were treated as follows. As a first step the cell voltage ( $\Delta V$ ) is corrected for the ohmic drop due to the resistance of the

wiring,  $R_{\text{wire}} = 0.8 \Omega$ . In a second step the current attributed to electronic conduction is subtracted from the acquired current. Values for the current due to electronic conduction are obtained by an extrapolation of the current measured below the thermodynamic potential of iron oxide decomposition given in Table III. The corrected current is labeled for simplification purposes  $i_{\text{EC}}$ . This current is then used to acknowledge the contribution of the electrolyte's resistance ( $R_{MO}$ ) in the electrochemical cell. The different steps can be summarized to

$$\Delta V_{\text{CIR}} = \Delta V - (i \times R_{\text{wire}}) - (i_{\text{EC}} \times R_{MO}) \quad [11]$$

Argumentation for this methodology is given in a previous study.<sup>[23]</sup>

#### D. Treatment of the Oxygen Signal

The performed complementary measurement of the anodically evolved gas is a powerful tool to interpret the occurring anode half-reaction. However, the  $\text{O}_2$ -analyzer is located far from the tip of the anode and, thus, produced oxygen is not synchronously measured with current. For the accurate interpretation of the oxygen signal in respect to the cell voltage, the measured  $\text{O}_2$  must be corrected for this registration delay.

In the experimental installation, the oxygen gas circuit consists of two different compartments, namely the travel time in the furnace-piping to the gas analyzer and the residence time of the gas within the electrochemical cell. A rough estimate on the travel time of  $\text{O}_2$  gas in furnace piping is calculated as follows:

$$t = \frac{s \times A}{Q} \quad [12]$$

where  $t$  is the travel time of the gas (hour),  $s$  the distance ( $\sim 6 \text{ m}$ ),  $A$  the transactional surface of the gas pipes ( $1.26 \times 10^{-5} \text{ m}^2$ ) and  $Q$  the volumetric gas flow rate ( $0.048 \text{ m}^3 \text{ h}^{-1}$ ). *Via* this estimate a travel time of 6 s is determined, which is negligible in comparison to the 600 s of each cell voltage increment. The  $\text{O}_2$  residence time in the electrochemical cell depends on several successive steps: (i) bubble nucleation; (ii) ascend of the bubble through the molten oxide layer; (iii) time of bubble floatation on the surface of the melt and (iv) a time to reach bubble saturation in the melt. The cumulative delay must be considered significant, as for example solely the bubble floatation on the surface of high viscous melts can last several minutes.<sup>[24]</sup> Hence, a delay correction must be performed to relate the measured oxygen signal with the current  $i$  and cell voltage  $\Delta V$ .

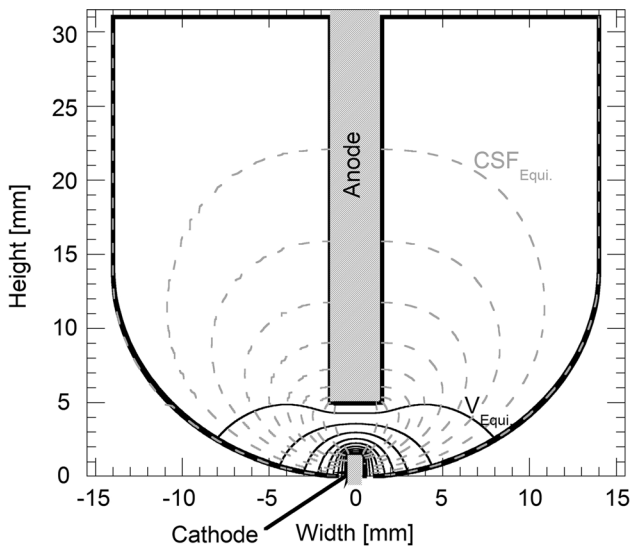


Fig. 2—The equipotential lines ( $V_{\text{Equi.}}$ ) and constant stream-function lines ( $\text{CSF}_{\text{Equi.}}$ ) in the electrochemical cell.

Table V. Calculated Conductivity  $\sigma_{MO}$  ( $\text{S cm}^{-1}$ ) at 1823 K of the Different Electrolyte Compositions in Dependence of  $\text{FeO}_x$  Concentration<sup>[18]</sup>

	Fe#0	Fe#1	Fe#2	Fe#3.5	Fe#5	Fe#7.5	Fe#8.75	Fe#10
$\sigma_{MO}$ ( $\text{S cm}^{-1}$ )	0.030	0.032	0.035	0.039	0.043	0.052	0.057	0.063

The determination of the delay in dependence of composition and current is done by supplementary cell voltage-pulse experiments. Here a cell voltage was applied for 30 minutes and the corresponding delay of O<sub>2</sub> registration determined. For each composition, the delay was identified for 1.5, 2, 2.5 and 3 V. Since during the SLSV the melt is constantly degassing O<sub>2</sub> gas, the cell voltage in the time in-between the different pulses was set to 1.2 V, which has proven sufficient to cause a continuous O<sub>2</sub> production. In Figure 3, a cell voltage pulse of 2 V is shown together with its O<sub>2</sub> response in electrolyte Fe#1. The delay of O<sub>2</sub> is 345 seconds. The measured delays for the different cell voltages are then fitted exponentially against the current values in the form of

$$t_D = ai^b \quad [13]$$

where  $a$  and  $b$  are constants,  $i$  is the measured current (mA) and  $t_D$  the time difference (seconds) between the cell voltage pulse and the first appearance of oxygen.

These fits, shown in Figure 4, are then used to correct the oxygen signal obtained in the SLSV concerning the registration delay. Therefore, the delay-time  $t_D$  is calculated based on current  $i$  measured at time  $t_{elec}$ . The sum of  $t_D$  and  $t_{elec}$ ,  $t_{O_2}$ , corresponds to the earliest time of measurement for oxygen evolved through a faradaic reaction at the anode.

$$t_{O_2} = t_{elec} + t_D \quad [14]$$

Current  $i$  is a direct result of the cell voltage application at time  $t_{elec}$ . Oxygen measured at time  $t_{O_2}$  has to be understood in the same manner. The voltammograms of the treated O<sub>2</sub> signal and treated cell voltage, see Section III-C, show therefore the corrected cell voltage,  $V_{CIR}$ , at  $t_{elec}$  vs the oxygen signal at time  $t_{O_2}$ .

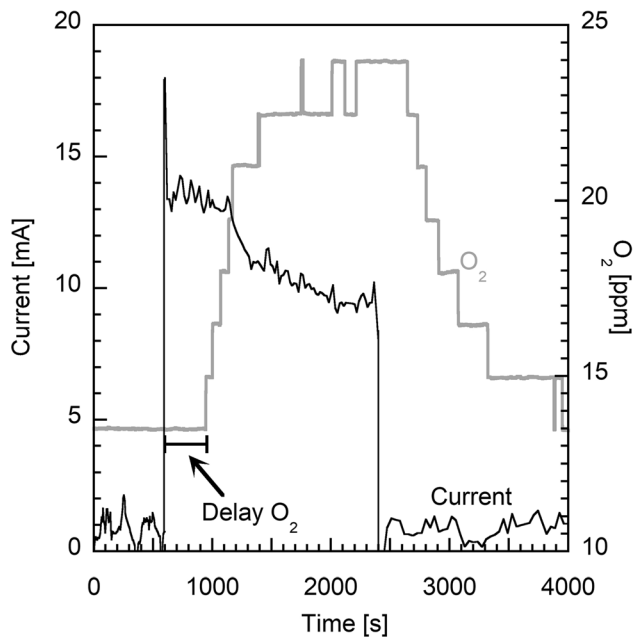
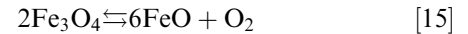


Fig. 3—Cell voltage pulse of 2 V in composition Fe#1 and the resulting oxygen signature; temperature: 1824 K ± 1, Ar-gas flow: 0.05 STP m<sup>3</sup> h<sup>-1</sup>.

In addition to this treatment, a background correction of the O<sub>2</sub> signal was performed to take into account the ongoing thermal decomposition of the iron oxides.



To do so, the O<sub>2</sub> signal acquired before O<sub>2</sub> production was extrapolated exponentially, yielding O<sub>2 Background</sub>, and then subtracted from the measured O<sub>2</sub> concentration, O<sub>2 meas</sub>.

$$O_{2BC} = O_{2meas} - O_{2Background} \quad [16]$$

O<sub>2BC</sub> then denotes the oxygen evolved by the faradaic reaction at the anode. Based on this value the Mol O<sub>2</sub> produced by the anode half-reaction (Mol O<sub>2 BC</sub>) is calculated. This is then used to determine the anodic yield, #O<sub>2</sub>, of the process following

$$\#O_2 = \frac{\text{Mol } O_{2BC}}{\text{Mol } O_{2100\text{pct}}} \quad [17]$$

where Mol O<sub>2 100 pct</sub> represents the number of mol O<sub>2</sub> produced by current  $i_{EC}$  assuming an ideal anodic yield.

### III. EXPERIMENTAL RESULTS

Voltammograms obtained in the different electrolytes are shown in Figure 5. Current augmented with increasing voltage and FeO<sub>x</sub> content, except for Fe#1 and Fe#2, which exhibited in this cell voltage range similar current values as Fe#0.

In the compositions Fe#0 to Fe#7.5 discontinuities of the current increase were observed in the voltage range 1 to 2.5 V. In contrast, the graphs of Fe#8.75 and Fe#10 increased monotonously.

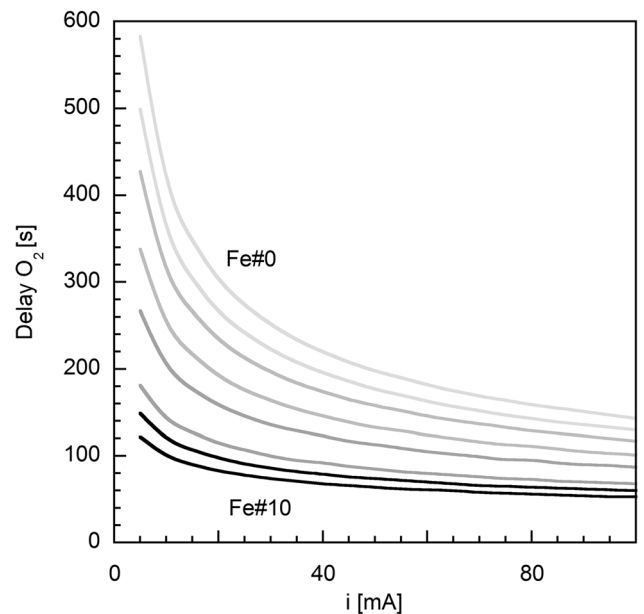


Fig. 4—Obtained exponential fits of the pulse experiments performed in the range of iron oxide concentrations investigated; temperature: 1824 K ± 4, Ar-gas flow: 0.05 STP m<sup>3</sup> h<sup>-1</sup>.

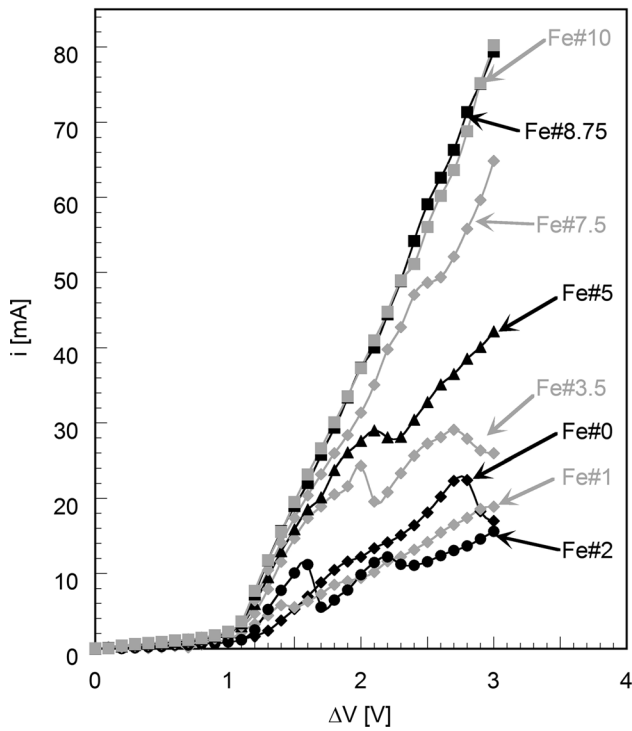


Fig. 5—Raw measured current during the linear scans (0 to 3 V); temperature: 1824 K  $\pm$  3, Ar-gas flow: 0.05 STP m<sup>3</sup> h<sup>-1</sup>, scanning rate 0.17 mV s<sup>-1</sup>.

Figure 6 shows the measured current below 0.9 V. The current measured in this cell voltage interval did not exceed 2 mA. A monotonous dependence of the current on the applied cell voltage is observed. It appears, however, that the concentration of iron oxide does not have a significant effect on the conduction in this voltage range.

Figure 7 shows the oxygen signals acquired during the trials. Below a cell voltage of  $\sim$  0.9 V the curves were characterized by a constant decrease. This is interpreted as a result of the ongoing thermal decomposition of the present iron oxide, Eq. [15]. The O<sub>2</sub> degassing rate dependence is consistent with the initial iron oxide concentration in the slag. The onset of oxygen production due to the faradaic reactions (*i.e.* iron reduction) occurred in the range of 1 to 1.7 V for all compositions. With increasing current and iron oxide content, the monitored O<sub>2</sub>-levels augmented.

#### IV. DISCUSSION

##### A. The Effect of Iron Concentration on the Electronic Conductivity of the Electrolyte

Electronic conduction describes the current flow due to an exchange of electrons between ferrous and ferric iron and depends on the iron oxide concentration. It is not linked to an electrochemical reaction in the cell. Thus, it has to be described separately from ionic conduction and the electrochemical reactions in the cell. The current transferred by electronic conduction in the

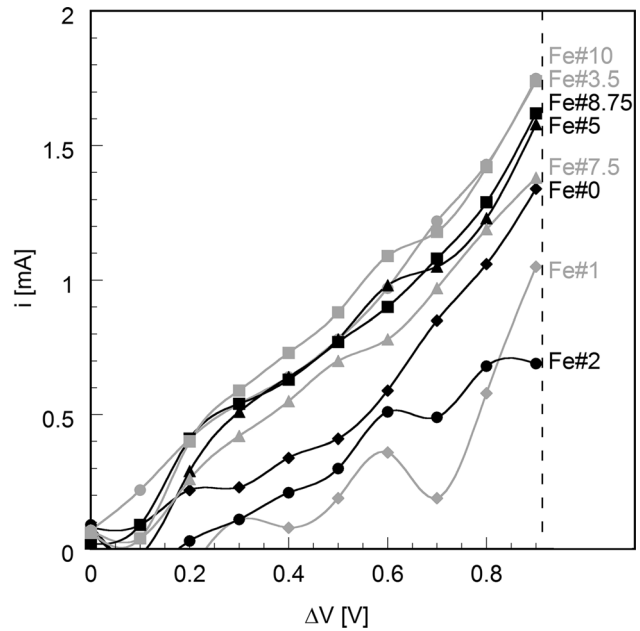


Fig. 6—Raw measured current in dependence of cell voltage (0 to 0.9 V); temperature: 1824 K  $\pm$  3, Ar-gas flow: 0.05 STP m<sup>3</sup> h<sup>-1</sup>, scanning rate 0.17 mV s<sup>-1</sup>.

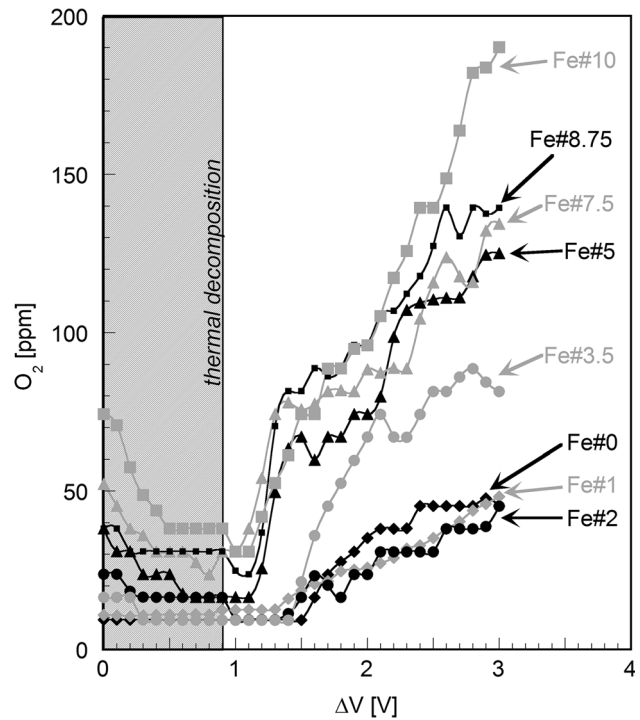


Fig. 7—Oxygen levels measured during linear scan voltammetry (0 to 3 V); temperature: 1824 K  $\pm$  3, Ar-gas flow: 0.05 STP m<sup>3</sup> h<sup>-1</sup>, scanning rate 0.17 mV s<sup>-1</sup>.

different electrolytes is directly measured at cell voltages below the thermodynamic threshold of reaction [3], the decomposition of ferrous iron oxide. The measured data, presented in Figure 6, show only a minor impact of the FeO<sub>x</sub> concentration on the current flow, which was not expected.

An estimate of the increase of electronic current due to the iron oxide addition can be given by Mott's equation,<sup>[13]</sup> assuming that the here unknown parameters, namely the phonon frequency and the wave function decay, are independent of the iron concentration and can thus be treated as constants. Doing so, the model suggests an increase of the charge transfer by the factor of 6 between composition Fe#1 and Fe#10. However, this model does not consider the electronic conductivity of the iron-free slag Fe#0. As seen in Figure 6, Fe#0 shows a charge transfer almost as high as Fe#10. The fact that this slag is conductive, diminishes the applicability of the model since it only considers the electron exchange between ferrous and ferric iron. The actual conductivity due to iron ions might be negligible and thus, a significant increase of the electronic conduction following the iron oxide concentration is not seen in the investigated compositional range.

As described in a previous study,<sup>[23]</sup> electronic conduction follows Ohm's law and can be estimated by linear extrapolation vs the cell voltage based on the current acquired below decomposition voltage of the different electrolyte compounds. Its percentage in respect to the measured current is shown in Figure 8 vs the applied cell voltage. In all compositions the electronic contribution decreases with increasing cell voltage. Only Fe#0 and Fe#3.5 deviate of this trend at elevated cell voltage, as for these compositions the measured current decreases throughout a limited voltage interval (see Figure 5). Also, the graph shows that the electronic contribution decreases with increasing iron content, indicating a disproportionate increase of the ionic conductivity in respect to the electronic

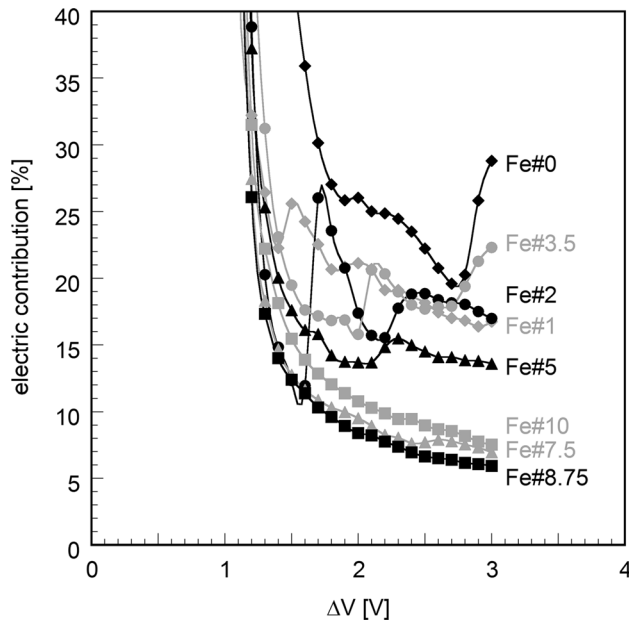


Fig. 8—Extrapolated electric fraction of the total measured current in dependence of cell voltage (0 to 3 V); temperature: 1824 K  $\pm$  3, Ar-gas flow: 0.05 STP m<sup>3</sup> h<sup>-1</sup>, scanning rate 0.17 mV s<sup>-1</sup>.

conductivity. For compositions  $\geq 7.5$  wt pct FeO<sub>x</sub> it is below 10 pct at 3 V, which indicates a high faradaic yield of the process.

### B. Results Corrected for Ohmic Drops and Delays

The measured current was treated by the ohmic drop correction proposed in Section III-C. To be able to compare the results with other studies, the current density  $j_{EC}$  is derived from the current  $i_{EC}$ . However, the deposition of liquid iron metal at the cathode during the SLSV must then be acknowledged. Production of the liquid metal leads to an increase of the cathode's surface, which might, therefore, impact the current density at the cathode. The significance of the cathode surface in respect to the current distribution can be evaluated by the Wagner number  $Wa$ ,<sup>[25]</sup> that is determined by

$$Wa = \frac{R_{kin}}{R_{MO}} \quad [18]$$

where  $R_{kin}$  is the kinetic resistance ( $\Omega$ ) of the electrode. Values for  $Wa \geq 5$  indicate uniform current distribution and at  $Wa \leq 0.2$ , the current distribution is nonuniform. For  $Wa \leq 0.2$ , only a small area of the electrode is important for the charge transfer and an increase of electrode surface is negligible. The kinetic resistance is dependent on the Tafel slope of the electrode reaction and the charge transfer. The Tafel slope for the reduction of ferrous iron in electrolytes Fe#5 and Fe#10 was defined in a previous study to 550 and 610 mV dec<sup>-1</sup>, respectively.<sup>[23]</sup> Below 50 mA the deposition of metal is deemed too small to change the electrode's surface. At 50 mA, the kinetic resistances in Fe#5 and Fe#10 are 18 and 22  $\Omega$ . In comparison, the electrolyte resistances at these iron oxide concentrations are 38 and 26  $\Omega$ . Derivation of the Wagner number following Eq. [18] for both concentrations gives values of 0.47 and 0.84. Therefore, it can be deduced that due to the high electrolyte resistance, the current distribution is nonuniform in these two cases. In consequence, the development of the cathode surface with iron metal production can be regarded as not important and it is thus unproblematic to derive the current density through division of the current by the calculated surface of the cathode wire, 5.5 mm<sup>2</sup>.

Figure 9 shows the linear scans after applying the ohmic drop correction and the conversion of the current  $i_{EC}$  into the current density  $j_{EC}$ . Onset of faradaic reaction in iron containing electrolytes is at approximately 1 V. The value of corrected cell voltage ( $\Delta V_{CIR}$ ) at the onset of current increase corresponding well with the calculated voltage of reaction [3], the decomposition of ferrous iron oxide. The possibility to decompose iron oxide at these conditions was shown in a study on the kinetics of liquid iron deposition in this molten oxide composition with 5 pct iron oxide.<sup>[23]</sup> As conditions of these two studies strongly resemble, it can be assumed that in the experiments presented here current flow is as well due to reaction [3].

The curves of Fe#8.75 and Fe#10 are straight vertical lines, indicating that no resistance linked to neither the electrode kinetics nor to mass transfer limit the flow of current between the electrodes. The maximum cathode current density observed is  $1.4 \text{ A cm}^{-2}$ . It should be noted that the corrected data for Fe#7.5 and Fe#8.75 exhibits a slight negative dependence between  $\Delta V_{\text{CIR}}$  and  $j_{\text{EC}}$ .

Conversely, curves of electrolytes Fe#1 and Fe#2 show a limitation of current flow between 1.1 and 1.3 V and 1.1 and 1.5 V, respectively. Furthermore, the amount of current in both compositions are similar to the measurement in Fe#0. Hence, in this range of concentrations dissolved, iron does not participate much in the transfer of current between the electrodes. Fe#3.5, Fe#5 and Fe#7.5 behave as intermediates, showing a limitation of the current flow but also a noticeable increase in comparison to the iron-free composition, Fe#0. The small inset of Figure 9 shows a magnification of the current limitation, marked as “Plateau”, detected in Fe#5.

These current discontinuities are an indication of a mass-transfer limitation. Most likely, the transfer limitation occurs at the cathode, due to its smaller surface compared to the anode. The average current density ( $j_{\text{lim}}$ ) of the different current plateaus is shown in Figure 10 vs with iron oxide concentration. The bars represent the maximum and minimum current density measured in each plateau.

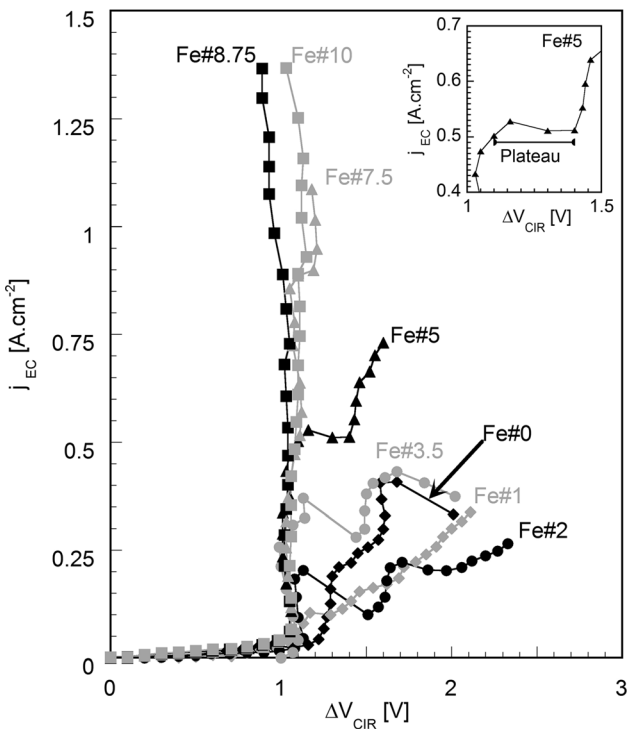
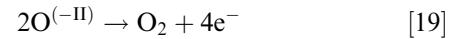


Fig. 9—Linear scans corrected by the leakage current, the wire resistance and the resistance of the slag; temperature:  $1824 \text{ K} \pm 3$ , Ar-gas flow:  $0.05 \text{ STP m}^3 \text{ h}^{-1}$ , scanning rate  $0.17 \text{ mV s}^{-1}$ .

The observed linear relationship confirms the presence of a mass-transfer limitation in compositions of the electroactive species, most likely  $\text{Fe}^{(\text{II})}$ . Following Fick’s law, the diffusion coefficient of the electroactive species does not change significantly when concentration and current are related linearly. The rate-limitation ends at roughly  $V_{\text{CIR}} = 1.5 \text{ V}$ , indicating the commence of reaction [5], the decomposition of  $\text{SiO}_2$  and the deposition of  $\text{Si}^{(0)}$  at the cathode. In Fe#7.5 this occurs at  $\Delta V_{\text{CIR}}$  of  $1.2 \text{ V}$ , which is a potential far too low for  $\text{SiO}_2$  decomposition. As mentioned above, however, this electrolyte exhibits a negative dependence of  $\Delta V_{\text{CIR}}$  on  $j_{\text{EC}}$ . Such a negative correlation might indicate that the used conductivity value is too low and the electrolyte’s resistance  $R_{\text{MO}}$  overestimated. In this case the derived  $\Delta V_{\text{CIR}}$  is smaller than the actual electrochemical potential. With augmentation of the current this would then lead to a decreasing  $\Delta V_{\text{CIR}}$ , thereby explaining the low voltage of the plateau’s upper boundary in composition Fe#7.5.

At the anode the charge transferring reaction is the oxidation of oxide anions following



This is confirmed by the corrected oxygen signal  $\text{O}_2_{\text{BC}}$  shown in Figure 11 vs the corrected cell voltage  $V_{\text{CIR}}$ .  $\text{O}_2$  production in iron oxide bearing composition starts at  $1 \text{ V}$  and follows the current density magnitude. As for the current density, values of Fe#0, Fe#1 and Fe#2 do not differ significantly, implying that the addition of iron oxide at these low concentrations has almost no effect on the charge transfer. Between Fe#8.75 and Fe#10 a distinct difference in magnitude of  $\text{O}_2$

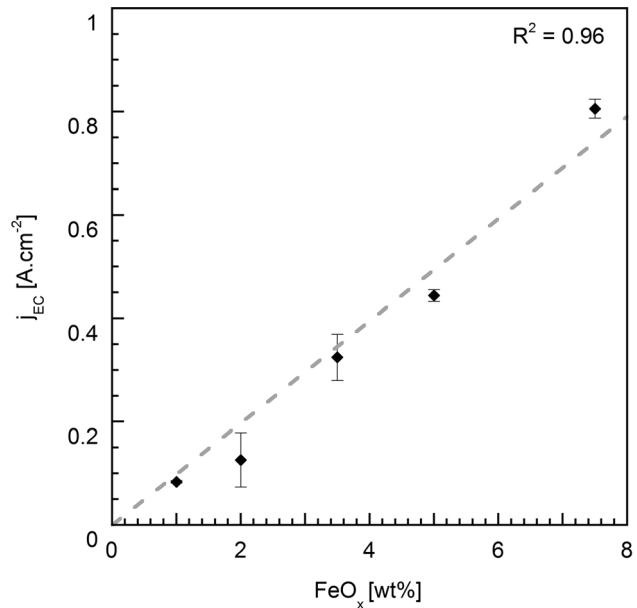


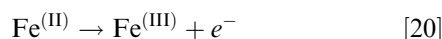
Fig. 10—The limiting current density of the different trials in dependence of the respective  $\text{FeO}_x$  concentration; the hachured line indicates a linear fit with 0 as origin; temperature:  $1824 \text{ K} \pm 3$ , Ar-gas flow:  $0.05 \text{ STP m}^3 \text{ h}^{-1}$ , scanning rate  $0.17 \text{ mV s}^{-1}$ .

production is observed, which stands opposed to the equal amount of current measured in both compositions (see Figure 9).

### C. Yield of $O_2$ Production

The efficiency of reaction [19] is given by the anodic yield which is calculated *via* Eq. [17]. Figure 12 shows the anodic yields obtained for compositions with  $\leq 3.5$  wt pct  $FeO_x$ .

For these electrolytes, a faradaic yield between 50 to 80 pct throughout the entire stepped linear scan voltammetry is observed. Considering the potential range 1 to 1.3 V, it is possible that oxygen gas produced at the anode remains entrapped in the molten oxide, due to the melt's high viscosity. At higher currents this artefact should not occur due to the buoyancy force of the increasing gas volume. However, the anode yield remains below 80 pct, which indicates that a second anodic reaction occurs, most likely the oxidation of ferrous iron into ferric iron *via*



Yet, the iron-free composition Fe#0 exhibits a similar anode yield as Fe#1-Fe#3.5. Since it does not contain iron the oxidation of ferrous iron cannot serve as explanation for the loss in anode yield in Fe#0. In reverse conclusion, the reason for the loss of anode yield in Fe#0 should occur as well in Fe#1-Fe#3.5 at cell voltages above 1.5 V in parallel to the oxidation of

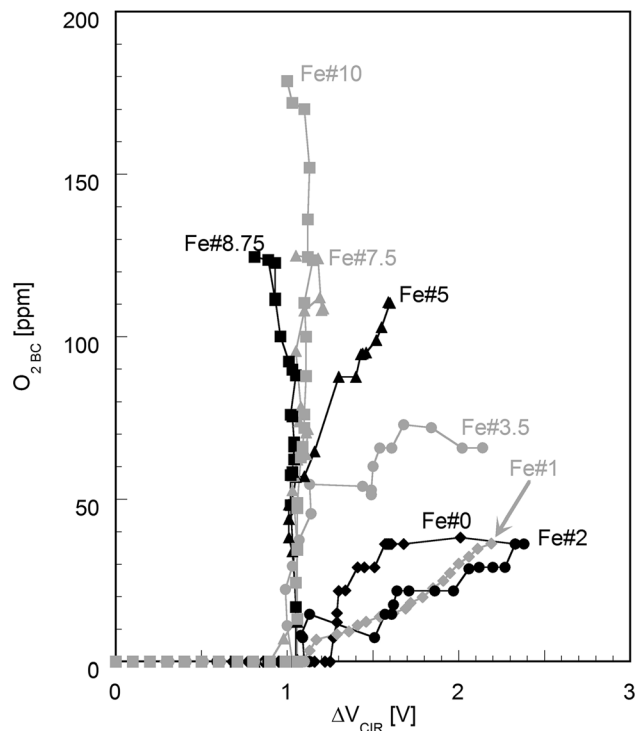
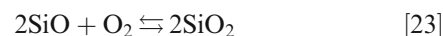
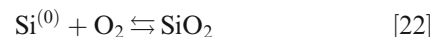
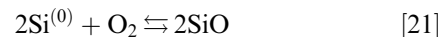


Fig. 11—Delay and background-corrected oxygen levels ( $O_2$  BC) vs the corrected cell voltage  $V_{CIR}$ ; temperature:  $1824 \text{ K} \pm 3$ , Ar-gas flow:  $0.05 \text{ STP m}^3 \text{ h}^{-1}$ , scanning rate  $0.17 \text{ mV s}^{-1}$ .

ferrous iron. However, the initial components in the Fe#0 cannot be oxidized any further and are unable to participate in the anode half-reaction.

In contrast, it is conceivable that a product of the cathode half-reaction reacts with the oxygen gas produced at the anode. Considering the reactions possible to occur in the iron free electrolyte, the reacting cathode products could be  $Si^0$  and  $SiO$ . Their oxidation by the anodically produced oxygen would follow:



The respective Gibbs energy of reactions [21] through [23] are  $-248$ ,  $-579$  and  $-662 \text{ kJ mol}^{-1}$ ,<sup>[20]</sup> confirming that these reactions would occur spontaneously.

Particular attention has to be attributed to reaction [23], as the compound is a gaseous phase at experimental conditions. The gas produced by the cathode half-reaction would rise through the electrolyte. Thus, the conditions for chemical reaction with the anodic produced  $O_2$  are given. Oxidation of the cathode product could occur either in the electrochemical cell or in the furnace piping. The anodic yield based exclusively on the electrochemical reaction at the anode would then be markedly higher as the here deduced values.

For the compositions Fe#5 to Fe#10, the respective anode yield is displayed in separate graphs in Figure 13. The anode yield in compositions Fe#5, Fe#7.5 and Fe#8.75 is characterized by values of  $\geq 100$  pct at the

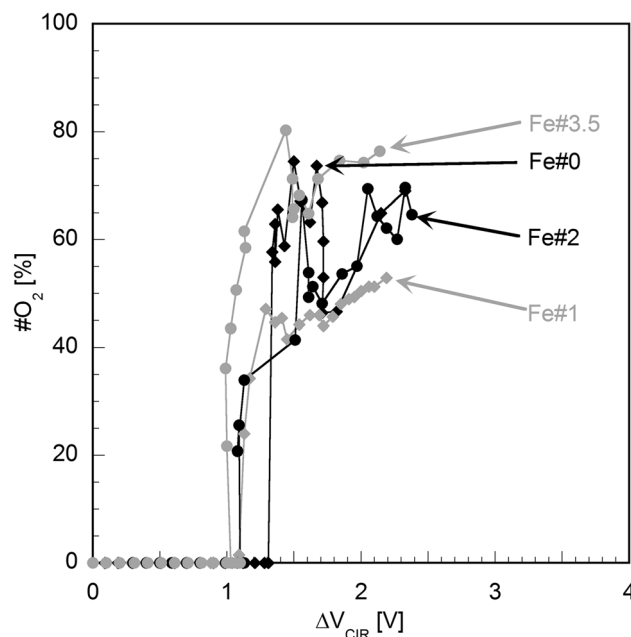


Fig. 12—Anodic yield in the compositions Fe#0, Fe#1, Fe#2 and Fe#3.5 in dependence of the cell voltage; temperature:  $1824 \text{ K} \pm 3$ , Ar-gas flow:  $0.05 \text{ STP m}^3 \text{ h}^{-1}$ , scanning rate  $0.17 \text{ mV s}^{-1}$ .

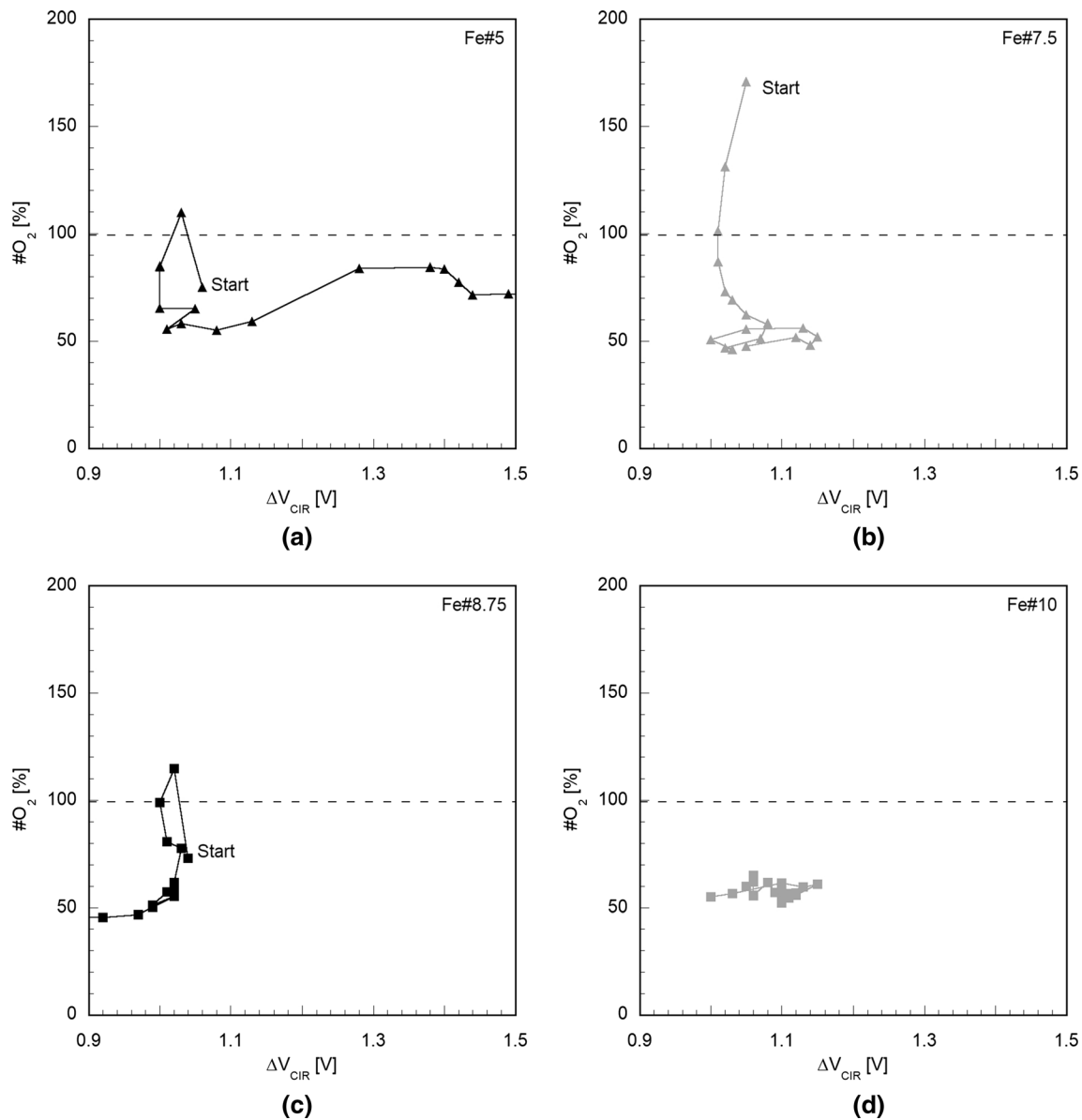


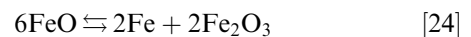
Fig. 13—Anodic yield in the compositions a Fe#5, b Fe#7.5, c Fe#8.75 and d Fe#10 in dependence of the cell voltage; temperature: 1824 K  $\pm$  3, Ar-gas flow: 0.05 STP m<sup>3</sup> h<sup>-1</sup>, scanning rate 0.17 mV s<sup>-1</sup>.

onset of the faradaic current. Values above 100 pct are considered as artifacts resulting from an underestimation of the quantity of O<sub>2</sub> released from thermal decomposition of iron oxide within the electrolyte. After this domain, the faradaic yield subsequently decreases in these three compositions and stabilizes for the remaining voltage interval between 50 and 70 pct. It is noteworthy that during the anode yield's decrease,  $\Delta V_{\text{CIR}}$  remains practically unchanged. Contrary to these three electrolytes, the composition Fe#10 shows a steady anodic yield of ~60 pct throughout the entire stepped linear scan voltammetry.

The anode yields around 100 pct in Fe#5 to Fe#10 indicate that the oxidation of oxide anions, reaction [19], can be the exclusive anode half reaction, which is coherent with results obtained elsewhere.<sup>[26,27]</sup> Then, the electroactive species is presumed to be free oxygen

anions.<sup>[28]</sup> However, with increasing voltage, the behavior of the molten oxide electrolyte changes, the anode yield decreases, which thus reveals the appearance of a second anode half reaction. Since the  $\Delta V_{\text{CIR}}$  of 1.5 V is not surpassed in all four electrolytes, reactions [21] through [23] cannot explain the loss in anode yield. Instead, it is possible that the increased iron concentration facilitates the oxidation of ferrous iron into ferric iron at the anode following reaction [20]

This tendency increases with increasing iron oxide concentration in the melt and explains the constant anodic yield of 60 pct obtained in composition Fe#10. The overall reaction in the electrochemical cell would then be described by



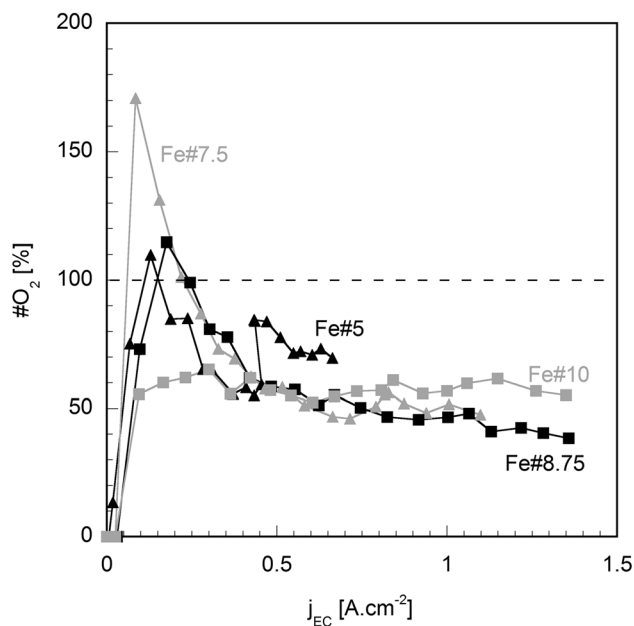


Fig. 14—Anodic yield in the compositions Fe#5, Fe#7.5, Fe#8.75 and Fe#10 in dependence of the faradaic current density; temperature: 1824 K  $\pm$  3, Ar-gas flow: 0.05 STP m<sup>3</sup> h<sup>-1</sup>, scanning rate 0.17 mV s<sup>-1</sup>.

The corresponding thermodynamic potential of this reaction in compositions Fe#1 and Fe#10, is 0.97 V and 0.81 V, respectively, which shows that the proposed reaction is thermodynamically feasible to occur. Furthermore, these potentials are below the values for decomposition of iron oxide into Fe-metal and O<sub>2</sub> gas, given in Table IV. However, the high anode yield observed in compositions Fe#5, Fe#7.5 and Fe#8.75 proves that conditions exist at which ferrous iron does not participate in the anode half-reaction, despite being thermodynamically favored.

Figure 14 shows the anode yield in comparison to the faradaic current density  $j_{EC}$ . It can be observed an anodic yield close to 100 pct is only obtained at current densities below 0.3 A cm<sup>-2</sup>. With further increase of the faradaic current density, the anode yield decreases in all compositions to values of 60 pct. This behavior implies a possible kinetic hindrance for the oxidation of ferrous iron which leads to a preference of free oxide anions for the electrochemical charge transfer at low current densities. This behavior is changed by the increase in iron oxide concentration to > 10 wt pct or current densities  $\geq$  0.3 A cm<sup>-2</sup>.

Despite the participation of ferrous iron, it is evident that compositions Fe#7.5 and Fe#8.75 exhibit a domain with an anode yield  $\sim$  100 pct, which is imperative for MIDEIO operation. The boundaries of this domain are specific to the iron oxide concentration and defined by the thermodynamic potential of iron oxide decomposition, *e.g.* Fe#8.75: 1.01 V, and the current density, *e.g.* Fe#8.75: 0.25 A cm<sup>-2</sup>.

## V. CONCLUSION

The molten oxide composition suggested in former work for MIDEIO of iron was investigated concerning its suitability for the process. An ohmic drop correction of the electrochemical signal was performed and the acquired current and O<sub>2</sub> signal were discussed in respect to the deduced operating voltage.

It was possible to show that the electronic contribution to the overall current decreases with augmentation of the iron oxide concentration in the investigated range of compositions indicating a high faradaic yield concerning the cathode half-reaction. It was furthermore observed that at concentrations below 5 wt pct, the addition of iron oxide has only a minor effect on the current flow in silicate melts. The detected mass transfer limitation at the cathode, associated with the diffusion of Fe<sup>(II)</sup>, can be understood as a confirmation of the limited impact of iron oxide in electrolytes with  $\leq$  7.5 wt pct FeO<sub>x</sub>. Above 7.5 wt pct FeO<sub>x</sub> the charge transfer at the cathode is only limited by the electrode kinetics.

Concerning the anode half-reaction, a two-case scenario is observed. In concentrations below 5 wt pct steady anode yields are observed in the range of 50 to 80 pct. The loss in efficiency is explained by a subsequent chemical reaction of the produced O<sub>2</sub> gas with the cathode products, Si<sup>(0)</sup> and SiO. In compositions with  $\geq$  5 wt pct FeO<sub>x</sub> a continuous sequence of occurring half-cell reactions is identified, involving oxide anions and ferrous iron. The consequence is the absence of a charge-transfer limitation in the anode half-reaction. Furthermore, it was inferred that the sequence of anode half reactions depends on the current density.

The results obtained in this study allow for the first time the description of working conditions for molten oxide electrolysis in silicate melts. The suitable potential range is then defined by the onset of iron oxide- and silica decomposition, thus 1 to 1.5 V. Concerning the oxygen gas production favorable conditions exist in dependence of the current density and iron oxide content. The maximum current density obtained at the cathode paired with a favorable anode yield is 0.25 A cm<sup>-2</sup> at a FeO<sub>x</sub> of 8.75 wt pct in the electrolyte.

## ACKNOWLEDGMENTS

The authors wish to acknowledge the French Agency for the Environment and Energy Management (ADEME) for the financial support.

## OPEN ACCESS

This article is distributed under the terms of the Creative Commons Attribution 4.0 International License (<http://creativecommons.org/licenses/by/4.0/>), which permits unrestricted use, distribution, and reproduction in any medium, provided you give

appropriate credit to the original author(s) and the source, provide a link to the Creative Commons license, and indicate if changes were made.

## REFERENCES

1. A. Allanore: *J. Electrochem. Soc.*, 2015, vol. 162, pp. E13–E22.
2. D.R. Sadoway: U.S. Patent; No. 5185068, 1993.
3. G.Z. Chen, D.J. Fray, and T.W. Farthing: *Nature*, 2000, vol. 407, pp. 361–64.
4. U.B. Pal: *J. Met.*, 2008, vol. 2, pp. 43–47.
5. G. M. Haarberg, E. Kvalheim, S. Rolseth, T. Murakami, S. Pietrzyk, and S. Wang: *ECS Trans.*, 2007, vol. 3, pp. 341–45.
6. Y. Gao, C. Yang, C. Zhang, Q. Qin, and G.Z. Chen: *Phys. Chem. Chem. Phys.*, 2017, vol. 19, pp. 15876–90.
7. Z. Zhou, H. Jiao, J. Tu, J. Zhu, and S. Jiao: *J. Electrochem. Soc.*, 2017, vol. 164, pp. E113–16.
8. D. Wang, A.J. Gmitter, J. Andrew, and D.R. Sadoway: *J. Electrochem. Soc.*, 2011, vol. 158 (6), pp. E51–54.
9. W.E. Haupin: *Essential Readings in Light Metals*, Springer, New York, 2016, pp. 3–11.
10. H. Kim, J. Paramore, A. Allanore, and D.R. Sadoway: *J. Electrochem. Soc.*, 2011, vol. 158, pp. E101–05.
11. A. Allanore, L. Yin, and D.R. Sadoway: *Nature*, 2013, vol. 497, pp. 353–57.
12. H. Inouye, J.W. Tomlinson, and J. Chipman: *Trans. Faraday Soc.*, 1953, vol. 49, pp. 796–801.
13. N. Mott: *Adv. Phys.*, 2001, vol. 50 (7), pp. 865–945.
14. M. Barati and K.S. Coley: *Metall. Mater. Trans. B*, 2006, vol. 37B, pp. 51–60.
15. L. Darken and R. Gurry: *J. Am. Chem. Soc.*, 1945, vol. 67 (8), pp. 1398–1412.
16. G. Ottonello, R. Moretti, L. Marini, and M.V. Zuccolini: *Chem. Geol.*, 2001, vol. 174, pp. 157–59.
17. ET Turkdogan: *The Physicochemical Properties of Molten Slags and Glasses*, The Metals Society, London, 1983.
18. J. Wiencke, H. Lavelaine, P.J. Panteix, C. Petitjean, and C. Rapin: *J. Appl. Electrochem.*, 2018, vol. 48 (1), pp. 115–26.
19. C. Gatellier, H. Gaye, J. Lehmann, and Y. Zbaczyniak: *Rev. Metall.*, 1992, vol. 89, pp. 887–88.
20. I. Barin: *Thermochemical Data of Pure Substances*, 3rd ed., Wiley, Hoboken, 2008.
21. J. Di Martino, C. Rapin, P. Berthod, R. Podor, and P. Steinmetz: *Corros. Sci.*, 2004, vol. 46, pp. 1849–64.
22. G. Georgalli, J. Eksteen, R. Bezuidenhout, B. Van Beek, T. Goff: Proc. 3rd Int. Platinum Conf., Platinum in Transformation, The Southern African Institute of Mining and Metallurgy, 2008. pp. 219–30.
23. J. Wiencke, H. Lavelaine, P.-J. Panteix, C. Petitjean, and C. Rapin: *Mater. Chem. Phys.*, 2018, vol. 212, pp. 214–23.
24. C. Nguyen, H. Gonnermann, Y. Chen, C. Huber, A. Maiorano, A. Gouldstone, and J. Dufek: *Geochem. Geophys. Geosyst.*, 2013, vol. 14 (9), pp. 3616–31.
25. A.D. McNaught and A. Wilkinson: *IUPAC. Compendium of Chemical Terminology, (the "Gold Book")*, Blackwell, Oxford, 1997, vol. 2.
26. A.H. Caldwell, E. Lai, A.J. Gmitter, and A. Allanore: *Electrochim. Acta*, 2016, vol. 219, pp. 178–86.
27. S.H. Lee and D.J. Min: *J. Electrochem. Soc.*, 2017, vol. 164 (8), pp. H5308–14.
28. A. Allanore: *Electrochim. Acta*, 2013, vol. 110, pp. 587–92.

**Publisher's Note** Springer Nature remains neutral with regard to jurisdictional claims in published maps and institutional affiliations.